Journal of Nuclear Materials 392 (2009) 40–44

Contents lists available at ScienceDirect

Journal of Nuclear Materials

journal homepage: www.elsevier.com/locate/jnucmat

Failure modes of vacuum plasma spray tungsten coating created on carbon fibre composites under thermal loads

T. Hirai [a,b,*], N. Bekris [a,c], J.P. Coad [a,d], C. Grisolia [a,e], J. Linke [a,b], H. Maier [a,f], G.F. Matthews [a,d], V. Philipps [a,b], E. Wessel [a,b]

[a] JET-EFDA, Culham Science Centre, OX14 3DB, Abingdon, UK
[b] Forschungszentrum Jülich EURATOM-Association, FZJ, D-52425 Jülich, Germany
[c] EFDA CSU, Culham Science Centre, Abingdon, Oxfordshire, OX14 3DB, UK
[d] Culham Science Centre, EURATOM-UKAEA Fusion Association, Abingdon, Oxfordshire, OX14 3DB, UK
[e] Association Euratom-CEA, Cadarache DSM/DRFC, F-13108, St-Paul-lez-Durance, France
[f] Max-Planck-Institut für Plasmaphysik, EURATOM Association, D-85748 Garching bei München, Germany

ARTICLE INFO

Article history:
Received 28 January 2009
Accepted 11 March 2009

PACS:
52.40.Hf
52.77.Fv
68.60.Dv
81.05.Mh
81.15.Rs

ABSTRACT

Vacuum plasma spray tungsten (VPS-W) coating created on a carbon fibre reinforced composite (CFC) was tested under two thermal load schemes in the electron beam facility to examine the operation limits and failure modes. In cyclic ELM-like short transient thermal loads, the VPS-W coating was destroyed sub-layer by sub-layer at 0.33 GW/m^2 for 1 ms pulse duration. At longer single pulses, simulating steady-state thermal loads, the coating was destroyed at surface temperatures above 2700 °C by melting of the rhenium containing multilayer at the interface between VPS-W and CFC. The operation limits and failure modes of the VPS-W coating in the thermal load schemes are discussed in detail.

1. Introduction

The primary ITER materials choice is a full beryllium (Be) main chamber wall with carbon fibre reinforced composite (CFC) at the strike points and tungsten (W) at the dome and the upper part of the divertor vertical targets. Neither the reference material combination (Be Wall/CFC + W divertor) nor its possible combination in the future (Be Wall/W divertor) have ever been tested in a tokomak. Therefore, the ITER-like Wall (ILW) Project has been launched at the JET tokamak [1,2]. The lessons we can learn from such an experiment in JET would be invaluable for reducing the risk of plasma-facing material related issues in ITER.

In the ILW Project, the JET tokamak will employ W-coated CFC tiles for the outer and inner divertor rows. For this application, a 200 μm thick vacuum plasma spray (VPS) W coating was selected at the end of the R&D program in 2006 [3–6]. During normal operation the W coating at the JET divertor will be exposed to intense transient heat loads as well as to steady-state thermal loads. Therefore, it is indispensable to assess the operation limits and failure modes of the coating under such thermal loading conditions.

In the present work, the operation limits and failure modes of the coating were studied under high thermal loads: (1) ELM-like short transient thermal loads; and (2) longer pulse loads simulating steady-state thermal loads in the electron beam facility.

2. Tungsten coating for thermal loading tests

The 200 μm W coating was produced by vacuum plasma spray technology [7] by Plansee AG. Thick coating was regarded to be advantageous since the major fraction of the heat dissipates in the thick coating before arriving at the interface during a short pulse. The characteristic heat propagation distance is considered

* Corresponding author. Present Address: ITER Organisation, Cadarache Centre, F-13108, St Paul-lez-Durance, France. Tel.: +33 4 42 25 65 35.
E-mail address: takeshi.hirai@iter.org (T. Hirai).

0022-3115/$ - see front matter © 2009 Elsevier B.V. All rights reserved.
doi:10.1016/j.jnucmat.2009.03.060

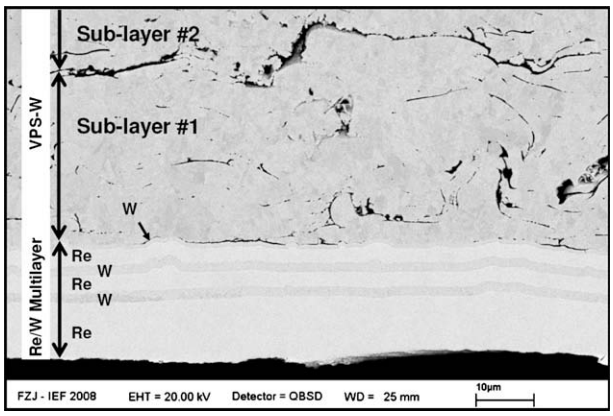

Fig. 1. Cross section of the VPS-W coating and the multilayer interlayer.

to be in a range of 100 μm during 1 ms assuming a lower thermal conductivity of the VPS-W coating than a solid W (e.g., the heat propagation distance in a solid W is estimated to be several hundreds μm in 0.5 ms [8]). Thus, the coating interface is not exposed to the thermal fatigue caused by the multiple short transient thermal loads. In fact, thinner W coatings (4 and 10 μm) were sensitive to such thermal loads since each heat pulse affected the interfaces [3,4].

The cross section around the coating interface is shown in Fig. 1. The W coating has a sophisticated interlayer consisting of a Rhenium (Re) and W multilayer. The Re/W multi-layer interlayer was aimed to be a diffusion barrier against carbon, preventing the formation of tungsten carbide in the main W coating [9,10]. The soft Re layers would also provide a compliant interface between the CFC and the hard W layers in the coating system. The multilayer interlayer was created by Physical Vapour Deposition (PVD) by alternating the deposition sources and processes, i.e., Re layers by arc deposition and W layers by sputtering deposition [11]. The multi-layer consisted of optimized six layers; 10 μm-Re, 2 μm-W, 3 μm-Re, 2 μm-W, 2.5 μm-Re and 1 μm-W, starting from the CFC surface to the VPS-W coating layer. The VPS-W coating was created in a vacuum at a high temperature; during the VPS process, the plasma torch delivers a power density in the order of 5 MW/m^2 onto the coating surface. The high process temperature can cause complicated residual stresses in the coating due to anisotropic thermal expansion mismatches between the W coating and CFC substrate. In addition, these residual stresses could cause tensile cracks in the W coating even just after production [6].

The W coating sample was produced on a two-directional CFC, (2D-CFC, DMS780 Dunlop). The CFC has a fibre-bundle architecture based on cross-ply laminates (*x*- and *y*-directions). PAN (polyacrylonitrile) fibre-bundles are utilized for the laminates. These fibre-bundles guarantee the high mechanical strength and thermal conductivity of the CFC in the two directions along the fibre-bundles. The carbon fibre-bundles have anisotropic thermal properties that originate from the nature of pyrolitic graphite [12] and the constituents [13]. Indeed, along the fibre direction, the thermal expansion is low (around 0–1 $\times$ 10^{-6} K^{-1}) and the thermal conductivity high, while in the fibre radial direction the thermal expansion is higher (10–13 $\times$ 10^{-6} K^{-1}) and the thermal conductivity lower. The CFC contains felt layers sandwiched between the two cross-ply laminates as a compliant layer. Both fibre-bundle layers and felt layers have typically about 0.5 mm thickness. The W coating was produced on a CFC surface containing perpendicular and parallel PAN fibre-bundles (Fig. 5(b)).

For the thermal tests, a large flat area of a CFC block which was roughly the half size of a JET divertor tile (G7 tile), 100 $\times$ 300 mm^2, was coated. It is worth mentioning that during VPS coating, the plasma torch moved across the surface to be coated from the starting point to end point and returned to the staring point [9]. During such a back and forth process, the atmosphere and substrate temperature have to be well controlled, especially for large surfaces; otherwise, sub-layers can be created by each pass of the plasma torch due to non-uniform stress and deposition of material from the halo of the plasma torch.

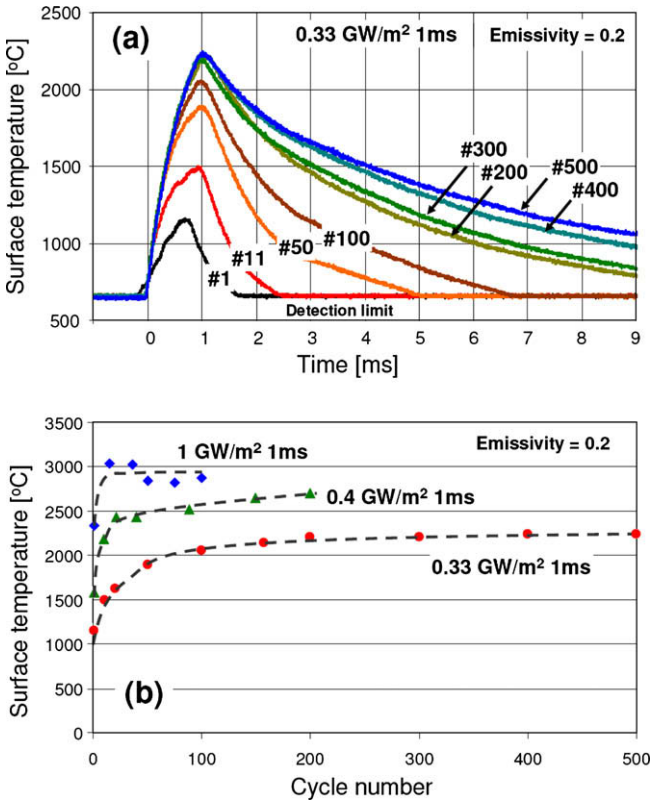

Fig. 2. (a) Time evolution of surface temperatures under thermal loads of 0.33 GW/m^2 for 1 ms over 500 pulses. Note that the data acquisition was triggered by a defined surface temperature level. Due to the slow temperature increase, the data acquisition of the first pulse started later. Therefore, the pulse duration of the first shot appeared to be short, although the pulse duration was the same as for the following shots. (b) Maximum surface temperature as a function of cycle number at the surfaces loaded at 0.33, 0.4, and 1 GW/m^2 for 1 ms.

3. High heat flux test in the electron beam facility JUDITH

High heat flux (HHF) tests were performed using the electron beam facility, JUDITH, at the Forschungszentrum Jülich, Germany [14,15]. The maximum beam power is 60 kW. The beam was focused to a diameter of approximately 1 mm. Fairly homogenous heat distribution is realized by fast scanning of the electron beam (typically 40 kHz in *x*-direction and 31 kHz in *y*-direction) at a well-defined area. The maximum beam scanning area is 100 $\times$ 100 mm^2 at the test position. Absorbed power density was calculated as the product of the acceleration voltage and the absorbed beam current. The acceleration voltage was held constant and the beam current was varied to provide defined heat loads. Although the acceleration voltage is high (120 kV), the penetration depth of the electron beam in solid tungsten was calculated to be up to 5 μm. Considering the thickness of the W coating (200 μm), the loading can be regarded as a surface heat flux.

ELM-like short transient thermal loading was applied by a 1 ms pulse with a rectangular waveform over a well-defined area of 16 mm^2 at room temperature. This load was repeated for 1000 cycles. The increase of bulk temperature of the W-coated CFC block

was negligible due to the large heat capacity of the CFC block. In these HHF tests, the power density limit and failure mode were examined.

Longer pulses were applied over an area of 64 mm^2 in order to simulate the steady-state heat load. It was necessary to limit pulse duration and the loading area to realize loads at high energy density and minimize the energy deposition into the sample. The pulse duration was selected to be 2 s which is much longer than the material time constant (characteristic time for heat propagation through the 200 μm thick W coating and interlayer to the CFC substrate, which is estimated to be in a range of several ms). The loaded area was designed to cover several pairs of cross-ply laminates of the underlying CFC laminate structure. Single pulse loads at virgin coating surfaces were applied at around room temperature. The bulk temperature increased up to 50 °C after the pules during the tests. In these HHF tests, the operational temperature limit and failure mode were examined.

The bulk temperatures were monitored with an infra-red camera, AGEMA THV900 (detection wavelength: around 3.5 μm) through a CaF_2 window. In addition, the time evolution of the averaged surface temperature in a 3–4 mm diameter spot was observed with a single colour pyrometer (detection wavelength: around 1.5–1.6 μm; detection limit 633 °C) though a quartz window. In both cases, the emissivity was assumed to be 0.2 over the measured temperature range.

4. Failure mode and power density limits of VPS-W coating under ELM-like short transient thermal loads

Fig. 2(a) shows the time evolution of surface temperature under heat loads of 0.33 GW/m^2 for 1 ms, over 500 cycles. As it is illustrated in this figure, the maximum surface temperature for the first shot was around 1200 °C. The maximum surface temperature increases with the number of shots and reaches 2200 °C after 200 shots. The maximum surface temperature increased drastically at the beginning of the cyclic loading and it saturated at a later stage (Fig. 2(b)). At higher power densities the temperature increase saturated at an earlier stage. This indicates the early completion of the coating destruction due to higher thermal stresses induced by higher power density loads. Another remarkable finding was a significant change of the cooling rates. After the first cycle, the surface temperature decreased rapidly, whereas after the 50th cycle, one can observe a noticeable slow down of the cooling rate. This indicates a poor thermal contact of the coating layers to the underlying substrate leading to a less efficient heat removal.

Fig. 3(a) shows the microstructure of the surface loaded at 1 GW/m^2 for 1 ms for 100 cycles. The coating showed surface damage that consisted of small droplets and peeling of sub-layers of the VPS-W coating. Numbers of cracks were generated at the loaded surfaces during the cyclic loading [16]. The sub-layers started to melt at the crack edges which had small local heat capacity. The micrograph (Fig. 3(a)) indicates the destruction processes: (i) cracking of an sub-layer, (ii) melting of crack edges of the sub-layer (marked as A), (iii) removal/extraction of the sub-layer due to melting/re-solidification of the molten sub-layer, (iv) cracking of the lower sub-layer due to thermal exposure (marked as B), and (v) melting of crack edges of the sub-layer (marked as C).

Fig. 3(b) and (c) show the cross section of the coating loaded at 0.4 GW/m^2 for 1 ms after 200 pulses. The coating was removed sub-layer by sub-layer due to the poor mechanical and thermal contact of each sub-layer. The VPS-W coating consisted of seven sub-layers as shown in Fig. 3(c). After removal/delamination of the sub-layers, melting of the sub-layer occurred because of the small heat capacity of the detached layers. Two sub-layers were removed after 200 cycles at 0.4 GW/m^2 for 1 ms loading as shown in Fig. 3(c). The same destruction process was observed after 500

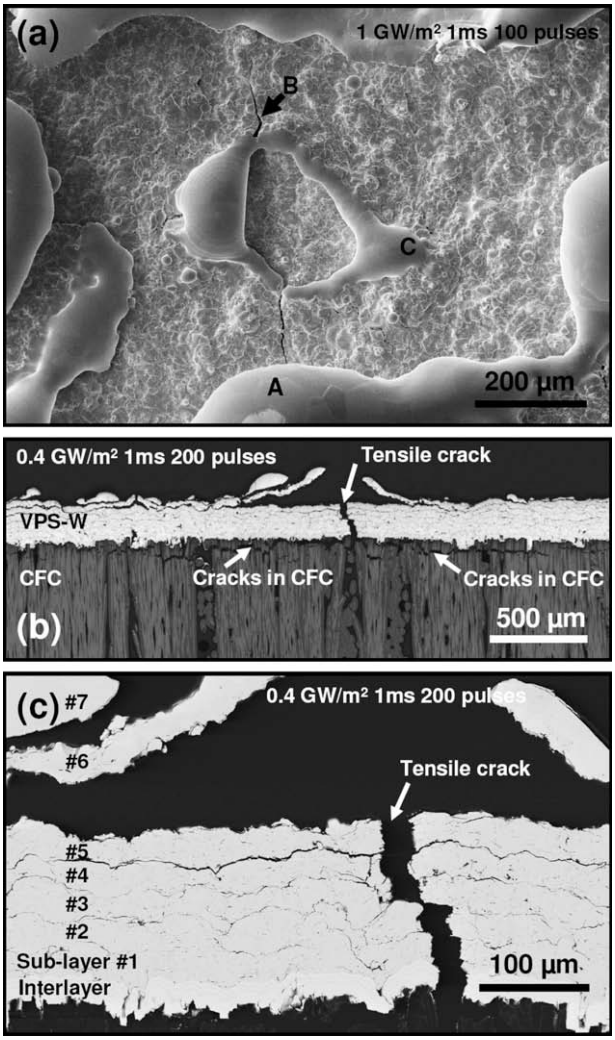

Fig. 3. (a) Microstructure of the loaded surface at 1 GW/m^2 for 1 ms over 100 cycles, (b) and (c) cross section of the loaded area at 0.4 GW/m^2 for 1 ms over 200 cycles.

cycles at 0.33 GW/m^2 for 1 ms. Fig. 3(b) and (c) also shows a tensile crack [6] which existed before the experiments, propagating through the entire VPS-W coating thickness and running across the loaded and non-loaded coating surfaces in perpendicular to the cross-ply fibre-bundle laminates of CFC. The tensile crack width in the image was around 20 μm.

The sub-layer structure in the VPS-W coating was not observed in the previous tests of 'small sample' (~80 mm × ~80 mm) which was prepared by the same technology as the large samples studied here. Indeed, the previous tests on the 'small sample' did not show any damage at 0.33 GW/m^2 for 1 ms over 1000 cycles [3]. The high resistance was likely associated with a monolithic structure of the thick coating without having sub-layers in the 'small sample'. It is concluded that the formation of the sub-layers during the production process was the critical point, which is assumed to be the result of scaling the process to large areas where deposition from the halo of the plasma torch and surface temperature are not as easy to control. In such VPS process, each sub-layer corresponds to a single pass of the plasma torch across the tile surface.

The multilayer did not show microstructural modification by this short pulse loading (Fig. 3(c)) since the coating was thermally thick, and therefore, the pulse duration was shorter than characteristic time which is estimated to be in a range of several ms for heat propagation through the coating to the interlayer. Thus, the coating

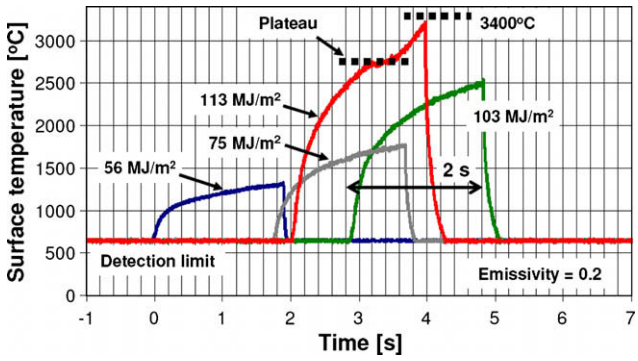

Fig. 4. Time evolution of the surface temperature during steady-state loads for 2 s.

interface was not strongly exposed to the thermal fatigue caused by the multiple short transient thermal loads.

Cracks developed horizontally in the CFC part were formed beneath the coating layer (Fig. 3(b)) due to poor mechanical stability. The cracks extended to a range of mm around the tensile cracks. These horizontal cracks caused an increase of the surface temperature and a low cooling rate because of the poor thermal contact.

5. Failure mode and temperature limits of VPS-W coating under steady-state thermal loads

Fig. 4 shows the time evolution of the surface temperature at the VPS-W coating during thermal loads at various energy densities. The coating was not damaged below 103 MJ/m^2 for 2 s [16]. The destruction occurred above 113 MJ/m^2 for 2 s. The measured averaged surface temperature at this energy density reached up to 3200 °C. As shown in the Fig. 4, the surface temperature showed a plateau at around 2700 °C (the temperature could be locally higher within the measured surface area). This plateau indicates melting of the coating. The temperature at the plateau was far below the melting temperature of W (3400 °C). This is due to melting of the interlayer after W–Re alloy and/or tungsten carbide formation, which would be created by mutual diffusion in the multilayer at high temperature. The melting points of the W–Re alloy and tungsten carbide go down to 2825 and 2715 °C, respectively [17]. This is the thermally weakest point in the coating system.

Fig. 5(a) shows a microstructure of the surface loaded at 113 MJ/m^2 for 2 s. At this energy density the coating showed melting. Two holes with a distance of about 2 mm were found at the loaded surface. CFC surfaces were found through the holes, which were caused by the poor wetting of the molten W alloy at the carbon surface. This separation between the two holes is due to the structure of the underlying CFC substrate as shown in Fig. 5(b). This microstructure implies that melting started at the multilayer interlayer around the CFC surface as discussed above. In the re-solidified layer at the top surface, W as well as small amounts of Re and C were detected by energy dispersive spectrometry (EDS) analysis [16].

The coating did not show any remarkable damage, e.g., melting, cracking, below 113 MJ/m^2 for 2 s [16]. It indicates that the coating had a clear damage threshold which is defined by the surface temperature. One must note that the threshold energy density is not relevant in this experiment since the energy dissipates in a large mass of the sample after being deposited at a small loaded area. Thermal loading at the entire sample surface was required to define the threshold energy density [18], which was not considered in these experiments.

Fig. 5(b) and (c) show cross sections of the damaged VPS-W coating. The section line was near the crater. The sectioning was

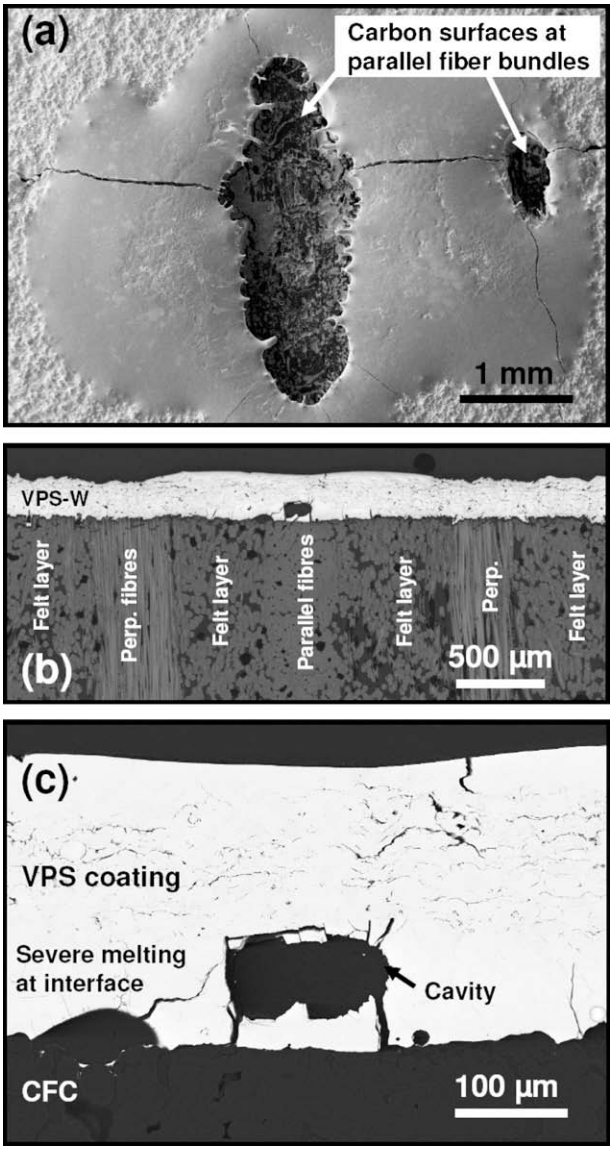

Fig. 5. Microstructure of the loaded area at 113 MJ/m^2 for 2 s, single pulse: (a) microstructure of the loaded surface; (b) and (c) cross section of the loaded area.

performed to include parallel and perpendicular fibre bundles in the cross section, namely, in parallel to the tensile crack shown in Fig. 5(a) and therefore the cracks did not appear in Figs. 5(b) and (c). As mentioned above, the melting of the coating depends on the underlying CFC structure. Fig. 5(b) shows that the coating melted at the fibre-bundle parallel to the surface where the heat transfer into the bulk was low. Here was the starting point of melting due to overheating. Severe melting was observed at the interlayer as shown in Fig. 5(c). Above the molten layer at around the interlayer, VPS-W sub-layers could still be observed and appear unaffected. This microstructure confirms that the destruction of the coating started by melting at the interlayer but not at the top surface. At the top surface, a re-solidified layer was observed, which originated from the surrounding crater near the section line. Consequently, the destruction processes of the coating under steady-state thermal loads are: (i) overheating at the parallel fibre-bundles of the CFC substrate; (ii) decrease of melting temperature by formation of W–Re alloy and/or tungsten carbide in the multilayer interlayer; (iii) melting of the interlayer; (iv) mass transport of molten phase during heating; and (v) a formation of cavities

during the cooling phase. The poor wetting of the molten W alloy at the carbon surface caused the large crater and open carbon surfaces at the damaged area.

6. Summary and concluding remarks

Thermal load tests were performed on a 200 μm thick VPS-W coating created on a 2D CFC with a W/Re multilayer interlayer. The thermal load tests were multiple short pulse loadings, i.e., ELM-like short transient thermal load tests, and longer single-pulse loading, i.e. steady-state thermal load tests.

Under ELM-like short transient thermal loads, the coating showed surface damage such as small droplets and peeling of sub-layers in the VPS-W layers. The damage threshold in power density was below 0.33 GW/m^2 1 ms. The formation of the sub-layers was the critical feature with respect to the performance of the VPS-W coating under the short thermal loads. Under steady-state thermal loads, the coating showed melting of the multilayer interlayer at the locally overheated parallel fibre-bundle surfaces. The formation of W–Re alloy and/or tungsten carbide caused decreases in the melting temperature of the coating. The damage threshold in operation temperature was found to be the melting points of the W–Re alloy and/or tungsten carbide, 2825 and 2715 °C, respectively.

As a result of numbers of experimental observations of failure of the thick W coatings under heat load tests, the ILW Project has decided to exclude the 200 μm VPS-W coating from the Project baseline. Thinner PVD-W coatings are being developed and are being qualified for the ILW Project [19].

Acknowledgements

Authors would like to thank Mr V. Gutzeit for his supports in the metallographic study of the coating. This work, supported by the European Communities under contract between Association EURATOM/FZJ, was carried out within the framework of the European Fusion Development Agreement. The views and opinions expressed herein do not necessarily reflect those of the European Commission.

References

[1] J. Pamela, G.F. Matthews, V. Philipps, R. Kamendje, JET-EFDA Contributors, J. Nucl. Mater. 363–365 (2007) 1.
[2] G.F. Matthews, P. Edwards, T. Hirai, M. Kear, A. Lioure, P. Lomas, A. Loving, C. Lungu, H. Maier, P. Mertens, D. Neilson, R. Neu, J. Pamela, V. Philipps, G. Piazza, V. Riccardo, M. Rubel, C. Ruset, E. Villedieu, M. Way, Phys. Scr. T128 (2007) 137.
[3] T. Hirai, H. Maier, M. Rubel, Ph. Mertens, R. Neu, E. Gauthier, J. Likonen, C. Lungu, G. Maddaluno, G.F. Matthews, R. Mitteau, O. Neubauer, G. Piazza, V. Philipps, B. Riccardi, C. Ruset, I. Uytdenhouwen, JET EFDA Contributors, Fusion Eng. Des. 82 (2007) 1839.
[4] H. Maier, T. Hirai, M. Rubel, R. Neu, Ph. Mertens, H. Greuner, Ch. Hopf, G.F. Matthews, O. Neubauer, G. Piazza, E. Gauthier, J. Likonen, R. Mitteau, G. Maddaluno, B. Riccardi, V. Philipps, C. Ruset, C.P. Lungu, I. Uytdenhouwen, JET EFDA Contributors, Nucl. Fusion 47 (2007) 222.
[5] R. Neu, H. Maier, E. Gauthier, H. Greuner, T. Hirai, Ch. Hopf, J. Likonen, G. Maddaluno, G.F. Matthews, R. Mitteau, V. Philipps, G. Piazza, C. Ruset, JET EFDA Contributors, Phys. Scr. T128 (2007) 150.
[6] H. Maier, R. Neu, H. Greuner, Ch. Hopf, G.F. Matthews, G. Piazza, T. Hirai, G. Counsell, X. Courtois, R. Mitteau, E. Gauthier, J. Likonen, G. Maddaluno, V. Philipps, B. Riccardi, C. Ruset, EFDA-JET Team, J. Nucl. Mater. 363–365 (2007) 1246.
[7] R.B. Heimann, Plasma Spray Coating: Principles and Applications, Wiley-VCH, Weinheim, 2008, ISBN 978-3-527-32050-9.
[8] T. Hirai, G. Pintsuk, Fusion Eng. Des. 82 (2007) 389.
[9] ITER Material Assessment Report 2001 G 74 MA 10 W0.3.
[10] H. Maier, Mater. Sci. Forum 475–479 (2005) 1377.
[11] H. Maier, J. Luthin, M. Balden, S. Lindig, J. Linke, V. Rohde, H. Bolt, ASDEX Upgrade Team, J. Nucl. Mater. 307–311 (2002) 116.
[12] B.T. Kelly, Physics of Graphite, Applied Science Publishers, 1981.
[13] G. Savage, Carbon–carbon Composites, first ed., Chapman and Hall, 1993.
[14] R. Duwe, W. Kühnlein, H. Münstermann, in: Proceedings of the 18th Symposium on Fusion Technology (SOFT), Karlsruhe Germany, 1994, 355–358.
[15] T. Hirai, K. Ezato, P. Majerus, Mater. Trans. 46 (2005) 412.
[16] T. Hirai, Study of Failure Modes of JET Tungsten Coatings under Multiple Transient Heat Loads and Steady State Loads, JW6-FT-3.35 Final Report, IEF2-TN/12-2008.
[17] T.B. Massalski, H. Okamoto, P. Subramanian, L. Kacprzak, Binary Alloy Phase Diagrams, ISBN0-87170-430-X, 1990, (William W. Scott, Jr.)
[18] T. Hirai, J. Linke, M. Rubel, J.P. Coad, J. Likonen, C.P. Lungu, G.F. Matthews, V. Philipps, E. Wessel, JET-EFDA Contributors, Fusion Eng. Des. 83 (2008) 1072.
[19] G.F. Matthews, J.P. Coad, H. Greuner, M. Hill, T. Hirai, J. Likonen, H. Maier, M. Mayer, R. Neu, V. Philipps, R. Pitts, V. Riccardo, ITER-like Wall Team, J. Nucl. Mater. 390–391 (2009) 934.